Available online at www.sciencedirect.com
SCIENCE DIRECT
Planetary and Space Science 54 (2006) 957–966
Planetary and Space Science
www.elsevier.com/locate/pss

Characteristics of dust particles detected near Saturn's ring plane with the Cassini Radio and Plasma Wave instrument

Z. Wang*, D.A. Gurnett, T.F. Averkamp, A.M. Persoon, W.S. Kurth

Department of Physics and Astronomy, University of Iowa, Iowa City, IA 52242, USA

Received 7 November 2005; accepted 4 May 2006

Abstract

During the inbound and outbound passes of the Cassini spacecraft through Saturn's ring plane on July 1, 2004, the Radio and Plasma Wave Science (RPWS) instrument detected many small particles striking the spacecraft. When a small particle strikes the spacecraft at a high velocity, it is instantly vaporized and produces a small cloud of plasma that expands radially outward from the impact site. As the plasma cloud expands away from the spacecraft it produces a voltage pulse on the RPWS electric field antennas, the amplitude of which is proportional to the mass of the impacting particle. Two types of measurements are made: waveform measurements from the *x*-axis dipole antenna, and spectrum measurements from the *w*-axis monopole antenna. The waveform measurements from the dipole antenna provide a determination of the impact rate and the relative mass distribution, and the spectrum measurements from the monopole antenna provide a determination of the root-mean-square particle mass. The impact rate at both ring plane crossings provides a good fit to the sum of two Gaussians, with an average impact rate of about 1200 per second (the exact value depends on the voltage threshold used), and a north–south thickness of about 300 km. The mass distribution depends on the distance from the ring plane, varying from about m^{-2} near the ring plane at $z = 0 \pm 100$ km, where z is the north–south distance from the ring plane, to as steep as m^{-4} well away from the ring plane at $z = 500 \pm 100$ km. The mechanisms involved in the impact detection are discussed and a formula relating the root-mean-square particle mass to the root-mean-square voltage on the *w*-axis monopole is derived. Using this formula, the root-mean-square mass is estimated to be 7.7×10^{-11} g, which for water ice particles with a density of 0.92 g cm^{-3} gives a root-mean-square radius of about 2.6 μm.

Keywords: Ring plane; Dust; Saturn

1. Introduction

It is well known that there are a large number of very small dust particles with sizes on the order of a few microns in the Saturn system (Smith et al., 1981; Esposito et al., 1984). These very small particles are primarily centered near the ring plane at a radial distance near and inside the G ring, and are most likely produced by micrometeoroid impacts on the rings and icy moons. The first direct detection of these small dust particles was with the radio and plasma wave instruments on the Voyager 2 spacecraft. During the Voyager 2 flyby of Saturn, numerous impulsive signals were detected by both the plasma wave and the planetary radio astronomy instruments as the spacecraft crossed the ring plane at a radial distance of $2.88R_S$ ($R_S = 60{,}268$ km), slightly outside of the G ring (Scarf et al., 1982; Warwick et al., 1982). Because the frequency spectrum extended well above the electron plasma frequency, which is the highest characteristic frequency of the plasma, it was concluded that the noise could not be due to plasma waves. From the impulsive waveform and the close proximity to the ring plane, Scarf et al. (1982) and Warwick et al. (1982) concluded that the signals were produced by the impacts of micron-sized particles hitting the spacecraft. The purpose of this paper is to use data from the Radio and Plasma Wave Science (RPWS) instrumentation on the Cassini spacecraft to investigate dust impacts during the first pass through the rings of Saturn, which occurred on July 1, 2004.

*Corresponding author.
E-mail address: zhenzhen-wang@uiowa.edu (Z. Wang).

0032-0633/$ - see front matter © 2006 Elsevier Ltd. All rights reserved.
doi:10.1016/j.pss.2006.05.015

The Cassini spacecraft, which was designed to investigate Saturn and its rings, moons, and magnetosphere, was launched on October 15, 1997, and placed in orbit around Saturn on July 1, 2004. Since it is the first orbiter of Saturn, it can provide much better spatial and temporal coverage than Voyagers 1 and 2. Two instruments on Cassini provide measurements of small dust particles: the cosmic dust analyzer (CDA) and the RPWS. The CDA is specifically designed to detect and analyze small dust particles (Srama et al., 2004), whereas the RPWS is mainly designed to study radio and plasma waves (Gurnett et al., 2004). Although the CDA has provided very useful surveys of micron and submicron dust particles in the outer regions of Saturn's rings (Kempf et al., 2005a, b), during the two very close passages through the rings at about $2.6R_S$ that occurred on July 1, 2004, the CDA was not operating. Thus, the RPWS provided the only measurements of dust particles in this crucial region, a region that probably will not be directly sampled again during the Cassini mission.

Compared with the Voyager plasma wave observations, several very significant improvements were made in the Cassini RPWS instrument that significantly enhanced the ability to detect and analyze dust impacts. First, the RPWS can operate the antenna elements both as a dipole and as a monopole. With this system, the charge released by dust impacts can be determined directly from the amplitude of the voltage pulse on the monopole antenna, thereby giving a signal that is proportional to the mass of the impacting dust particle. Second, the dynamic range of the RPWS antenna voltage waveforms was increased from 4-bit resolution to 8-bit, thereby making it possible to obtain mass distributions from a pulse height analysis of the observed impact waveforms. In addition, an on-board microprocessor algorithm can be used to continuously identify and analyze dust impacts throughout the mission. More details about RPWS on Cassini can be found in Gurnett et al. (2004).

2. Observations

Fig. 1 shows the trajectory of the Cassini spacecraft during the first encounter with Saturn. The spacecraft passed northbound through the ring plane between the F and G rings on the inbound pass and southbound between the same two rings on the outbound pass. The inbound ring plane crossing occurred at 00:46:32 Universal Time (UT) on July 1, 2004, at a radial distance of $2.634R_S$ ($R_S = 60{,}268$ km), and the outbound ring plane crossing occurred at 04:33:51 UT on the same day at a radial distance of $2.630R_S$.

The RPWS instrumentation consists of three electric field antennas, three search coil magnetic antennas, a Langmuir probe and its associated electronics, and five specialized receivers. In the dust detection mode, only the high frequency receiver and the wideband receiver are used. The configuration of the electric field antennas and their orientation with respect to the x, y, and z axes of the spacecraft are shown in Fig. 2. In the mode of operation used for detecting dust impacts during the July 1, 2004, ring plane crossings, the wideband waveform receiver was configured to respond to the voltage difference between the E_U and E_V antennas (hereafter called the x-axis dipole). At both ring plane crossings very intense impulsive signals were detected in the wideband receiver waveforms, with the maximum intensity occurring very close to the center of the ring plane. Fig. 3 illustrates the wideband voltage waveform obtained during the first ring plane crossing. The sample rate during this pass was such that the time between samples is 36 μs. Some representative dust impact waveforms are shown by the arrows. The dust impact waveforms typically exhibit a very rapid rise on a time scale of a few tens of a microsecond, followed by a complicated recovery waveform. The rise time is controlled by the bandwidth of the receiver, which is 10 kHz. The total duration of the initial pulse typically lasts less than 1 ms, followed by a longer second peak of opposite polarity that lasts for several milliseconds. Most of the pulses fall well within the dynamic range of the receiver. In the gain state that most commonly occurred during the ring plane crossings pulses with an antenna voltage up to about ± 65 mV can be detected. Above this amplitude the pulses are clipped.

To count dust impacts, abrupt steps in the x-axis antenna voltage are identified by requiring that two successive pairs of voltage measurements have slopes of the same sign, either positive or negative. If the total voltage change between the first and last of the three points exceeds 1.6 mV then the step is counted as a dust impact. The 1.6 mV detection threshold was selected on a trial-and-error basis so that it is just above the background noise level at the ring plane crossing. Once an impact is identified, the computer software introduces a dead time of 252 μs during which no further impacts are recognized. This dead time is introduced to avoid spurious transient effects that are sometimes introduced during the complicated recovery waveform. Once the impacts have been identified the impact rate R is computed by counting the number of impacts over a given time interval, after correcting for the dead time. The counting interval is usually about 125 ms, but can vary from as little as 52 ms to as much as 272 ms depending on onboard computer software limitations. The impact rate obtained using this procedure is shown versus time in UT in Fig. 4 for the inbound ring plane crossing and in Fig. 5 for the outbound ring plane crossing. A scale at the bottom of these figures also shows the z position of the spacecraft measured positive north from the Saturn's equatorial plane. For both ring plane crossings the impact rate reached a maximum value very close to the equator ($z = 0$) and has a quasi-Gaussian dependence on the distance z from the equatorial plane. As with a similar study of dust impacts by Tsintikidis et al. (1994) using the Voyager 2 data, we find that the sum of two Gaussians

$$R = R_0 + R_1 e^{-(z-h)^2/L_1^2} + R_2 e^{-(z-h)^2/L_2^2}, \quad (1)$$

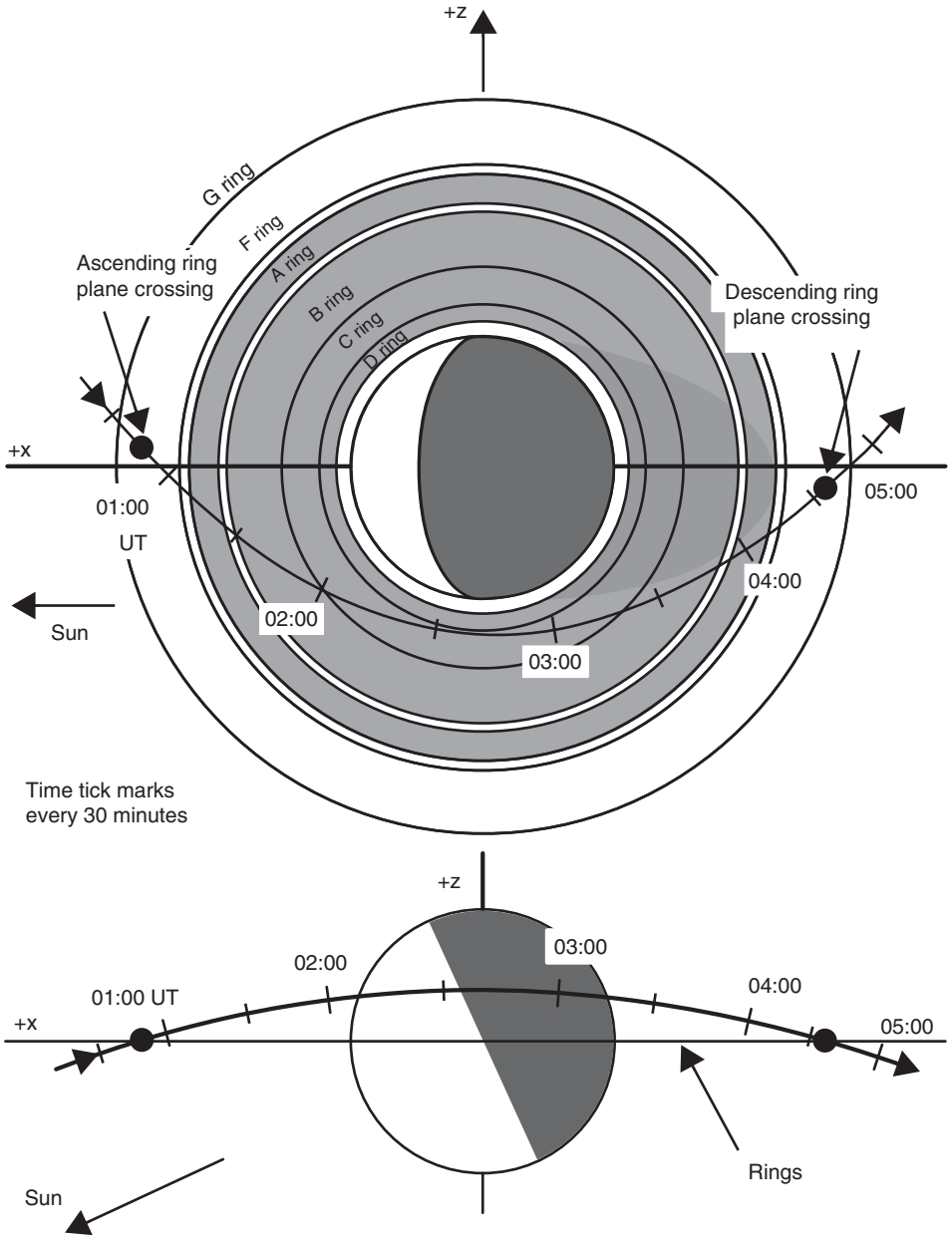

Fig. 1. The trajectory of the Cassini spacecraft as it passed through the rings of Saturn on July 1, 2004.

gives a good fit to the impact rate profile, where h is the offset from the equatorial plane and L is the half-thickness of the respective Gaussian component. The optimum values of the fit parameters listed in Figs. 4 and 5 were obtained by minimizing the goodness of fit parameter $\chi^2 = \sum(R_i - R)^2/(N-6)$, where N is the total number of data points and 6 is the number of free parameters in Eq. (1). The impact rate from the Gaussian fit reaches a maximum value of $1164\,s^{-1}$ for the inbound ring plane crossing and $1262\,s^{-1}$ for the outbound crossing.

The number density of the impacting particles can be derived from the impact rate R using the equation

$$R = nUA, \tag{2}$$

where U is the relative speed between the spacecraft and the dust particles and A is the effective cross-sectional area of the spacecraft body. The relative speed between the spacecraft and the particles, which are assumed to be in circular Keplerian orbits around Saturn, was $16.6\,km\,s^{-1}$ for the inbound ring plane crossing and $15.9\,km\,s^{-1}$for the outbound ring plane crossing. Since the spacecraft was oriented during both crossings such that the high gain antenna protected the main body of the spacecraft from impacts (see Fig. 2), the effective area for dust impacts is dominated by the high gain antenna. From the 4 m diameter of the high gain antenna (Matson et al., 2002) the effective cross-sectional area is estimated to be $A = 12.6\,m^2$. Using this area, the relative velocities, and the best fit impact rates at the inbound and

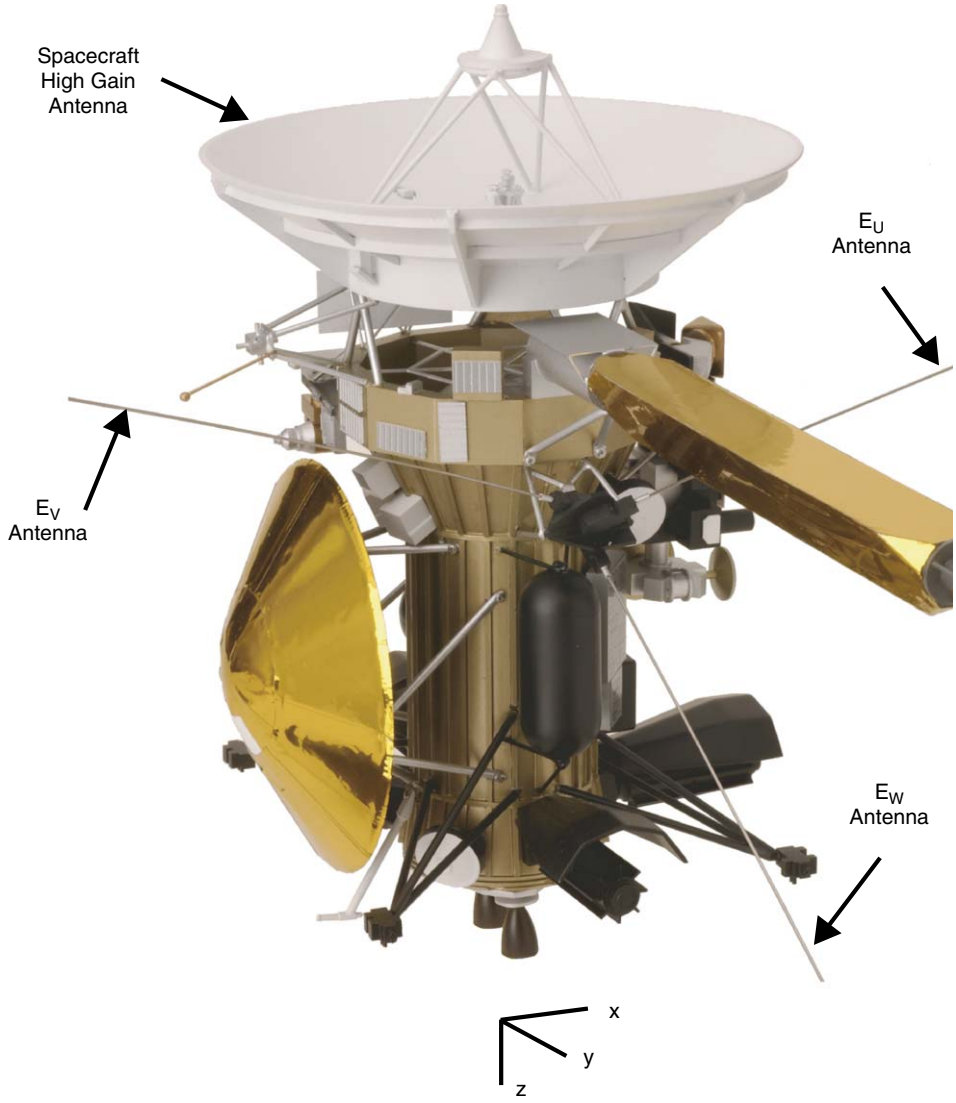

Fig. 2. A sketch of the Cassini spacecraft showing the locations of the RPWS antennas and their relationship to other structures on the spacecraft. During the inbound and outbound ring plane crossing that occurred on July 1, 2004, the spacecraft orientation was such that most of the impacts occurred on the spacecraft high gain antenna.

outbound ring plane crossing, which are 1164 and 1262 s^{-1}, respectively, the average number densities given by Eq. (2) are 5.57×10^{-3} and $6.31 \times 10^{-3}\,m^{-3}$, respectively. Recent comparisons with dust measurements in the E ring by the Cassini CDA suggest that the effective area for dust detection by the RPWS maybe significantly smaller than the area of the high gain antenna (Kurth et al., 2006). If this proves to be correct, then the average number densities computed above will have to be increased by the appropriate factor.

In the Gaussian fit given by Eq. (1), L_1 represents half of the north–south thickness of the "core" dust distribution and L_2 represents half of the north–south thickness of the less dense "halo" surrounding the core. For the inbound ring plane crossing, the north–south thickness of the core component is $2L_1 = 296$ km and the north–south thickness of the halo component is $2L_2 = 714$ km. For the outbound ring plane crossing, the north–south thickness of the core is $2L_1 = 320$ km and the thickness of the halo is $2L_2 = 726$ km, both of which are very similar to the inbound crossing.

Since the amplitude of the voltage pulse on the antenna is believed to be proportional to the mass of the impacting particles (Gurnett et al., 1983; Aubier et al., 1983), the mass distribution of the dust particles can be determined from the amplitude distribution of the voltage pulses on the antenna. For each impact the maximum voltage amplitude on the x-axis dipole antenna during the 252 μs dead time interval was computed relative to the voltage that existed immediately before the impact. To compute the pulse amplitude distribution, the voltage amplitudes were sorted into the 0.5 mV bins and the number of the impacts in each bin was counted for a specific time interval. By dividing by

the total number of impacts, the fraction of impacts per bin, $F(V)$, versus peak voltage of dust impacts can then be obtained. Fig. 6 shows $F(V)$ near the center of the first ring plane crossing ($-70\,\text{km} < z < 70\,\text{km}$). Since the pulse amplitude is expected to be proportional to the mass of the impacting particle, this plot gives the mass distribution of the dust particles, $\mathrm{d}N/\mathrm{d}m$. The exact voltage-to-mass conversion given at the bottom of the plot will be discussed in the next section. The fractional voltage amplitude distribution in Fig. 6 has been plotted on a log–log plot so that a power-law distribution appears as a straight line. As can be seen, above about 1 mV, which is the approximate background noise level, the differential mass distribution $\mathrm{d}N/\mathrm{d}m$ varies approximately as m^{-2}. Note that some particles almost certainly exist below the detection threshold. Therefore, the number densities described previously only represent a lower limit. To investigate how the mass distribution depends on z the amplitude distribution of the peak voltages observed well away from the center of the first ring plane crossing is shown in Fig. 7 for $-565\,\text{km} < z < -425\,\text{km}$, and in Fig. 8 for $425\,\text{km} < z < 565\,\text{km}$. As can be seen the mass distribution away from the ring plane is notably steeper than the mass distribution near the center of the ring plane, varying more like $\mathrm{d}N/\mathrm{d}m \sim m^{-4}$. The increase in the slope of the mass distribution indicates that there are proportionally fewer large particles in the region well away from the center of the ring plane compared to the region near the center of the ring plane. Another notable feature in Figs. 7 and 8 is a very prominent step-like decrease in the mass distribution at a voltage of about 8 mV. This step-like decrease occurs both north and south of the ring plane (compare Figs. 7 and 8), but is not present on the outbound pass where the slope is more nearly independent of z. Apparently, this is a local feature not present at all points around the ring.

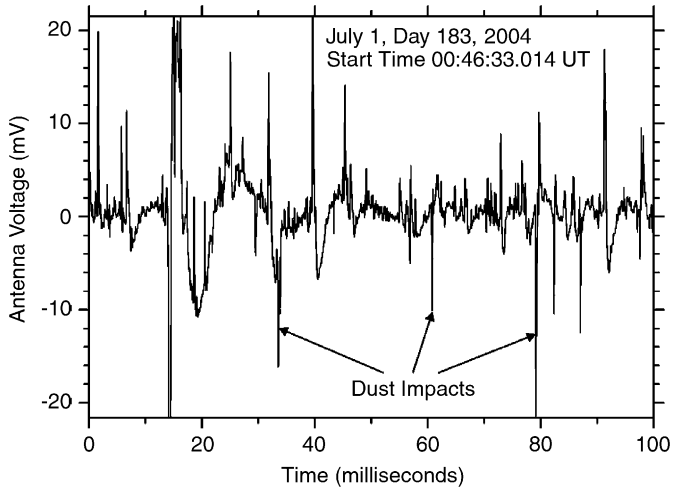

Fig. 3. The wideband voltage waveform obtained from the $E_U - E_V$ electric dipole antenna during the first ring plane crossing. Some representative dust impact waveforms are shown by the arrows.

In addition to the distribution of voltage amplitudes, $F(V)$, it is also of interest to compute the root-mean-squared (r.m.s.) voltage, V_{rms}, which will be used in the

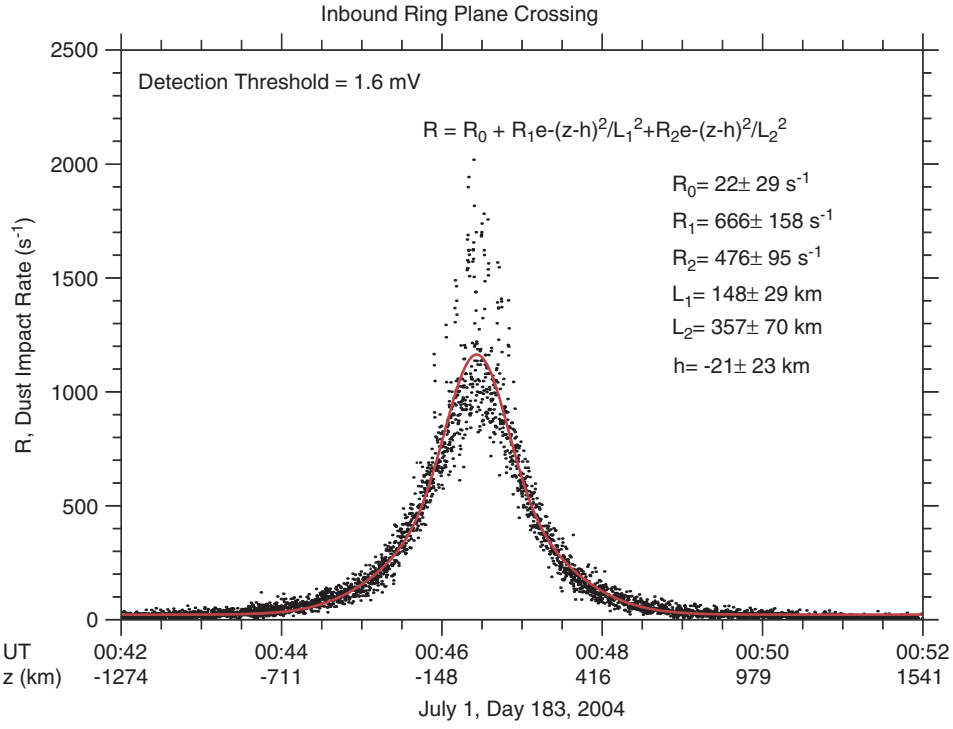

Fig. 4. The impact rate R versus Universal Time (UT) and north–south distance z from the equatorial plane of Saturn for the inbound ring plane crossing. The best fit sum of two Gaussian curves is also shown by a red solid line.

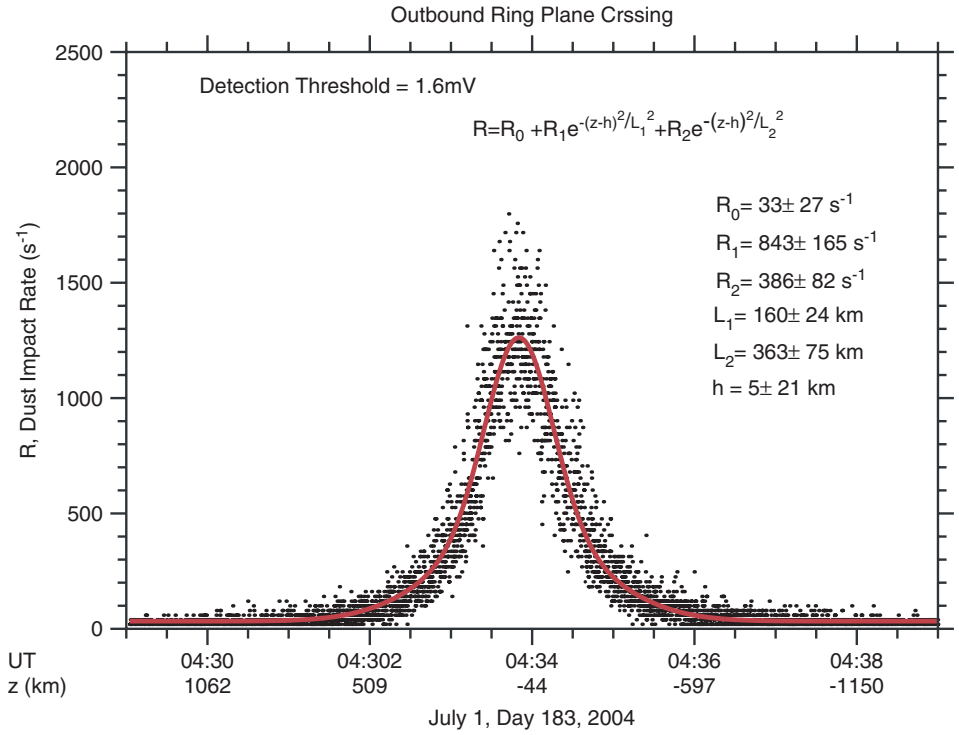

Fig. 5. The impact rate R versus the time in UT and height z from the equatorial plane of Saturn for the outbound ring plane crossing. The best fit for a sum of two Gaussian curves is shown by the red solid line.

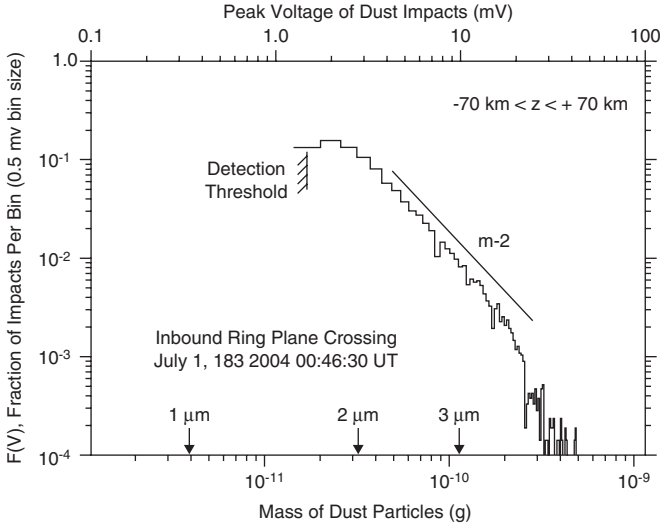

Fig. 6. The amplitude distribution of the peak voltage of dust impacts observed near the center of the first ring plane crossing ($-70\,\text{km} < z < 70\,\text{km}$). The fraction of impacts per bin, $F(V)$, is proportional to the differential mass distribution, $\mathrm{d}N/\mathrm{d}m$, and the peak voltage of dust impacts is proportional to the mass of the dust particles. Above about 1 mV, the differential mass distribution $\mathrm{d}N/\mathrm{d}m$ varies approximately as m^{-2}.

next section to compute the r.m.s. mass of the dust particles. For purposes of computing V_{rms}, it is useful to plot $V^2F(V)$, so that we can judge whether there is enough dynamic range available to give an accurate determination of the r.m.s. voltage. Fig. 9 shows a plot of $V^2F(V)$ near the center of the first ring plane crossing ($-70\,\text{km} < z < 70\,\text{km}$). The r.m.s. voltage squared, V^2_{rms}, is given by the area under the curve. It is evident that the area under the curve is reasonably well determined, since there does not appear to be a large contribution from impacts that are either above or below the available dynamic range (i.e., less than about 1.6 mV, or greater than about 65 mV). The r.m.s. voltage near the ring plane, from $-70\,\text{km} < z < 70\,\text{km}$, computed by integrating under the curve is $V_{\text{rms}} = 6.65\,\text{mV}$.

Since the voltage measured by the dipole antenna depends somewhat on the location of the impact, the best way to characterize the absolute voltage spectrum of the dust impacts is by measuring the voltage on the monopole antenna. Since the monopole gives the voltage between the antenna and the spacecraft body, this voltage is expected to be independent of the location of the impact. Fig. 10 shows the voltage spectral density on the monopole as obtained from the low-rate spectrum analyzer near the center of the ring plane crossing ($-70\,\text{km} < z < 70\,\text{km}$). The voltage spectral density has been plotted on a log–log plot so that a power-law distribution appears as a straight line. For low frequencies (below about 4000 Hz), the spectral density is proportional approximately to f^{-2}, and as predicted by the theory of Aubier et al. (1983) at high frequencies (above about 4000 Hz), the spectral density is proportional approximately to f^{-4}.

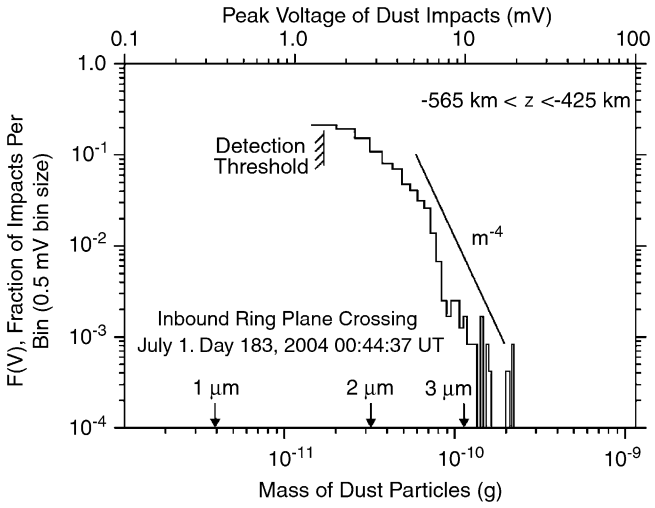

Fig. 7. The amplitude distribution of the peak voltages of dust impacts observed south of the first ring plane crossing, at $-565\,\mathrm{km} < z < -425\,\mathrm{km}$. Above about 1 mV, the differential mass distribution $\mathrm{d}N/\mathrm{d}m$ varies approximately as m^{-4}, indicating that there are proportionally fewer large particles in this region, compared to the region near the center of the ring plane.

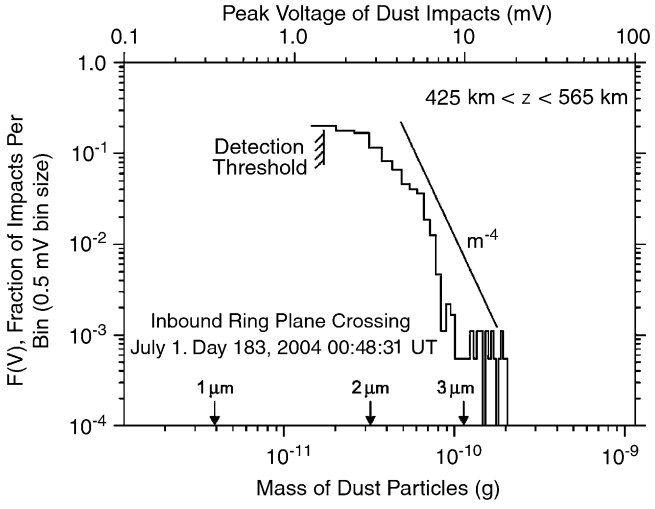

Fig. 8. The amplitude distribution of the peak voltages of dust impacts observed north of the center of the first ring plane crossing, for $425\,\mathrm{km} < z < 565\,\mathrm{km}$. Note the very close similarity to Fig. 7, including the step-like decrease at about 8 mV.

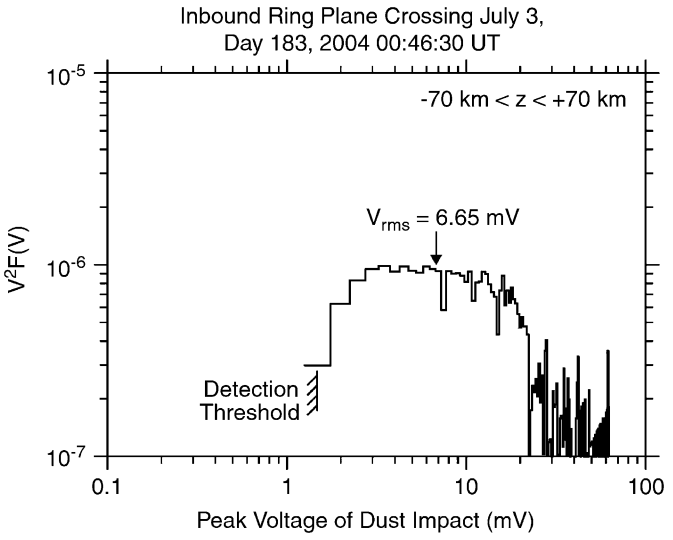

Fig. 9. The mass distribution of dust particles near the center of the first ring plane crossing for $-70\,\mathrm{km} < z < 70\,\mathrm{km}$. The quantity $V^2F(V)$ represents the contribution of dust particles to the total r.m.s. voltage, and therefore to the total r.m.s. mass. Note that most of the contribution to the total r.m.s. voltage lies well within the dynamic range of the instrument at this gain setting, i.e., from about 1.6 to 65 mV.

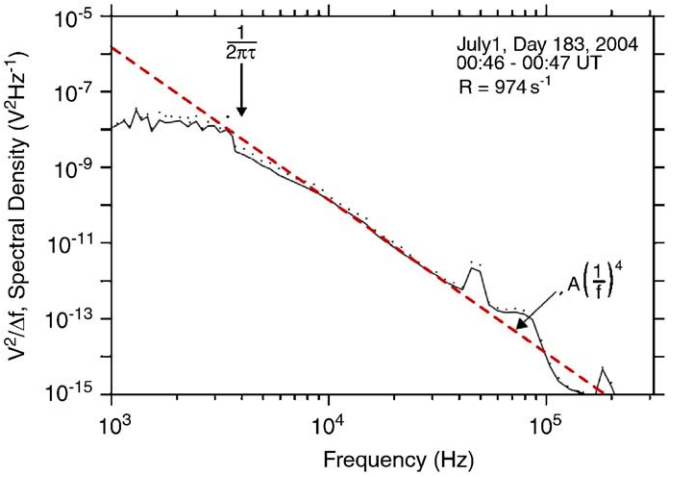

Fig. 10. The voltage spectral density of the dust impacts detected by the monopole antenna near the center of the first ring plane crossing. The spectrum varies approximately as f^{-2} at frequencies lower than 4000 Hz and as approximately f^{-4} at frequencies higher than 4000 Hz. The change in slope at $f_c = (1/2\pi\tau)$ provides a useful parameter for estimating the particle mass, and the red line gives the best fit to the f^{-4} part of the spectrum.

3. Root-mean-square mass

Fig. 11 illustrates what happens when a small high-velocity particle traveling at a speed of many kilometers per second strikes the surface of the spacecraft. Upon impact the kinetic energy of the particle is converted into heat which vaporizes both the particle and part of the target material, thereby producing a small partially ionized cloud of gas. Some of the electrons $(-Q)$ in this rapidly expanding plasma cloud escape leaving the spacecraft body with a charge Q. Laboratory measurements show that the charge released is proportional to the mass of the impacting particle, i.e., $Q = km$, where k is a constant that depends on the speed of the particle. The mass-to-charge conversion constant k has been measured for various materials and impact velocities in the laboratory by Grün (1981), and is approximately $k = 0.4\,\mathrm{C\,g^{-1}}$ for dielectric particles (such as water ice) striking a metal target at a speed of $16\,\mathrm{km\,s^{-1}}$, which is typical of the impact velocities that occur at the Cassini ring plane crossings. It should be noted that laboratory measurements are not available for the target material (conducting paint) that is actually present on the high gain antenna, so the above value for the

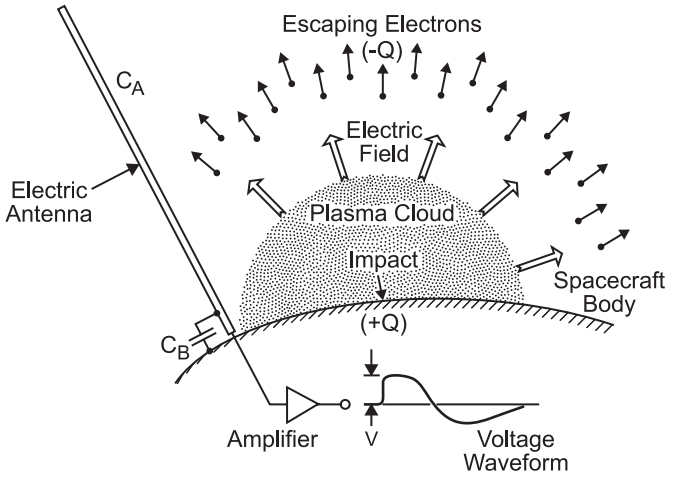

Fig. 11. An illustration showing the plasma cloud and the escaping electrons ($-Q$) produced by an impact on the spacecraft body, and the resulting polarization charge ($+Q$) on the spacecraft body. The escaping electrons produce a polarization electric field that is detected by the antenna. The resulting antenna voltage is $V=\beta Q/C$, where C is the capacitance of the spacecraft and $\beta\approx 0.4$ is a factor that takes into account the voltage reduction caused by the base capacity of the antenna.

charge-to-mass conversion constant is at best an intelligent guess, and could very well be in error by a substantial factor. After the impact, the escaping electrons cause a nearly radial electric field to develop in the plasma cloud between the spacecraft body and the escaping electrons. It is this polarization electric field that induces the voltages in the electric antennas. On Cassini the antenna voltage can be measured by the RPWS in two ways: via waveform measurements using the x-axis dipole antenna, and via spectrum measurements using the w-axis monopole antenna. Since the voltage induced on the dipole antenna involves a differential measurement, which is inherently sensitive to the impact location, the best way to estimate the mass of the impacting particle is by measuring the voltage on the monopole antenna, which is directly related to the charge Q remaining on the spacecraft body.

As the plasma cloud expands over the monopole antenna, the high frequency receiver detects a voltage pulse, Q/C, that is related to the effective capacity C of the spacecraft body. The capacity of the spacecraft body is estimated to be about $C=200$ pF (Gurnett et al., 2004). As a simple model, the voltage on the monopole antenna can be represented by the following waveform (Aubier et al., 1983):

$$V(t)=0, \quad t\leqslant 0,$$

and

$$V(t)=(1-\mathrm{e}^{-t/\tau})(Q/C)\beta, \quad t>0, \tag{3}$$

where τ is the rise time of the impact ionization process and $\beta\approx 0.4$ is a factor that takes into account the voltage reduction due to the known base capacity of the antenna, i.e. $\beta=C_A/(C_A+C_B)$, where $C_A\approx 100$ pF is the antenna capacity and $C_B\approx 150$ pF is the base capacity (see Fig. 11).

It is easy to show that the Fourier transform of $V(t)$ is

$$V(\omega)=\frac{Q}{C}\left(-\frac{1}{\mathrm{i}\omega}+\frac{1}{\mathrm{i}\omega-1/\tau}\right)\beta. \tag{4}$$

The voltage spectrum is then given by

$$V^2=|V(\omega)|^2=\frac{Q^2\beta^2}{C^2\omega^2}\left(1-\frac{1}{1+1/\tau^2\omega^2}\right). \tag{5}$$

For low frequencies, $\tau^2\omega^2\ll 1$, the term $1/(1+1/\tau^2\omega^2)$ is much less than 1 and can be neglected compared to 1. Thus, at low frequencies the spectral density is proportional to f^{-2}, i.e.

$$V^2=\frac{Q^2\beta^2}{C^2\omega^2}=\frac{Q^2\beta^2}{(2\pi)^2C^2f^2}. \tag{6}$$

For high frequencies, $\tau^2\omega^2\gg 1$, the spectral density function simplifies to

$$V^2=\frac{Q^2\beta^2}{C^2\tau^2\omega^4}=\frac{Q^2\beta^2}{(2\pi)^4C^2\tau^2f^4} \tag{7}$$

and the spectral density is then proportional to f^{-4}. As shown in Fig. 10 the voltage spectral density on the monopole antenna has a very good fit to this expected f^{-4} frequency dependence. Taking $\tau^2\omega_c^2=1$ as defining the critical frequency that distinguishes the low frequency region from the high frequency region, we can obtain the rise time τ. From Fig. 10 one can see that the critical frequency, $f_c=(1/2\pi)\omega_c$, is approximately 4000 Hz. The corresponding rise time is then $\tau=40\,\mu$s.

Since the charge Q released by the impact is directly proportional to the mass of the impacting particle, after substituting $Q=km$ into Eq. (7) it is easy to see that the voltage spectrum caused by one dust impact is given by

$$V^2=\frac{k^2m^2\beta^2}{(2\pi)^4C^2\tau^2f^4}. \tag{8}$$

Next we show that by measuring the voltage spectrum of many impacts, we can obtain the r.m.s. mass distribution of the dust particles. Integrating from the minimum mass to the maximum mass of the detected dust particles, we can compute the r.m.s. mass, which is given by

$$m_{\mathrm{rms}}=\sqrt{\langle m^2\rangle}=\sqrt{\frac{1}{N}\int_{m_{\min}}^{m_{\max}}\frac{\mathrm{d}N}{\mathrm{d}m}m^2\,\mathrm{d}m}, \tag{9}$$

where N is the total number of particles. Similarly, we can compute the r.m.s. voltage, which is given by

$$V_{\mathrm{rms}}=\sqrt{\langle V^2\rangle}=\sqrt{\frac{1}{N}\int_{m_{\min}}^{m_{\max}}\frac{\mathrm{d}N}{\mathrm{d}m}V^2\,\mathrm{d}m}. \tag{10}$$

Comparing these two equations with Eq. (8) we see that the relationship between the r.m.s. voltage and the r.m.s. mass is given by

$$V_{\mathrm{rms}}^2=\frac{k^2m_{\mathrm{rms}}^2\beta^2}{(2\pi)^4C^2\tau^2f^4}. \tag{11}$$

Since the voltage spectral density is the average voltage spectrum produced by one impact, we must multiply the above equation by the impact rate, R, to obtain the voltage spectral density produced by many impacts. The voltage spectral density produced by an impact rate R is then given by

$$\frac{V_{\rm rms}^2}{\Delta f} = \frac{Rk^2 m_{\rm rms}^2 \beta^2}{(2\pi)^4 C^2 \tau^2 f^4} = A\left(\frac{1}{f}\right)^4, \quad (12)$$

where A is a coefficient that can be computed from the measured voltage spectral density. The parameters that we have adopted for computing the r.m.s. mass are as follows: $C = 200\,\text{pF}$, $\tau = 40\,\mu\text{s}$, $k = 0.4\,\text{C g}^{-1}$ and $\beta \approx 0.4$. The average impact rate for the spectrum in Fig. 10 is $R = 974/\text{s}$. Substituting these parameters into Eq. (12) and canceling the common $(1/f)^4$ terms then gives the following relationship between the coefficient A and the r.m.s. mass

$$A = 2.5 \times 10^{26}\,\text{m}_{\rm rms}^2\,V^2\,\text{Hz}^2. \quad (13)$$

The coefficient A can be obtained by fitting a straight line to the f^{-4} spectrum in Fig. 10. This spectrum can be described by the following equation:

$$\log\left(\frac{V^2}{\Delta f}\right) = \log(Af^{-4}) = -4\,\log f + \log(A), \quad (14)$$

By evaluating one point from this line, we obtain

$$A = 1.5 \times 10^6 V^2\,\text{Hz}^2. \quad (15)$$

Substituting this value of A into Eq. (13) then gives

$$m_{\rm rms} = 7.7 \times 10^{-11}\,\text{g}. \quad (16)$$

This result shows that the r.m.s. mass of dust particles near the ring plane is on the order of a few times 10^{-11} g, a result that is similar to previous work by Aubier et al. (1983) for the Voyager 2 ring plane crossing. Assuming that the dust particles are made of water ice, which has a density of $0.92\,\text{g cm}^{-3}$, the corresponding r.m.s. particle radius is 2.6 μm, i.e., on the order of a few microns.

4. Discussion and conclusions

In this paper, we have described and analyzed the dust impacts detected by the Cassini RPWS during the first pass through Saturn's ring plane. Although the Cassini and Voyager 2 ring plane crossings occurred in different parts of the ring system and the instrumental parameters are somewhat different, the peak number densities are quite similar. The number densities at the two Cassini ring plane crossings at 2.634 and $2.630 R_S$, are slightly smaller, 5.6×10^{-3} and $6.3 \times 10^{-3}\,\text{m}^{-3}$, but still very similar to the number density ($15 \times 10^{-3}\,\text{m}^{-3}$) given by Tsintikidis et al. (1994) for the Voyager 2 ring plane crossing. Also the north–south impact rate profiles for both the Cassini and Voyager 2 ring plane crossings fit the sum of two Gaussians, thereby indicating the presence of "core" and "halo" components. The fit parameters are, however, somewhat different. For the Cassini crossings the north–south thickness, $2L_1$, of the "core" component was about 300 km, compared to 962 km for the "core" component during the Voyager 2 ring plane crossing (Tsintikidis et al., 1994) and the north–south thickness of the "halo" component was about 700 km, compared to 3376 km for the "halo" component during the Voyager 2 ring plane crossing.

Because of the improved dynamic range and the availability of simultaneous measurements from both dipole and monopole antennas, the Cassini RPWS instrument has a much better capability than the Voyager plasma wave instrument for determining the mass distribution of the impacting particles. Using the impact coupling model developed by Aubier et al. (1983), we developed a formula that describes the relationship between r.m.s. voltage detected by the monopole antenna and the r.m.s. mass. Using this relationship, the r.m.s. mass of the dust particles near the inbound ring plane crossing was estimated to be 7.7×10^{-11} g. A similar value was obtained for the outbound ring plane crossing. Assuming that the dust particles are water ice with a mass density of $0.92\,\text{g cm}^{-3}$, the corresponding r.m.s. radius is 2.6 μm. This estimate of the size of the particle depends critically on the assumed mass-to-charge conversion constant, which from the best available data was assumed to be $k = 0.4\,\text{C g}^{-1}$. Because of the current lack of laboratory data for the likely target material on the high gain antenna, this value could very well be in error by a substantial factor. However, we note that the particle radius only depends on the cube root of the mass-to-charge conversion constant, so even an error factor of ten would only change the estimated radius of the particles by a little more than a factor of two. So it is clear that the typical radius of impacting particles is on the order of a few microns. From the distribution of voltage amplitudes we also showed that the mass distribution of the impacting particles detected near the ring plane decreased with increasing mass, varying approximately as m^{-2} near the ring plane. As the distance from the ring plane increased the slope of the mass distribution tends to increase, varying approximately as m^{-4} at a distance of 500 km from the ring plane during the inbound ring plane crossing. This north–south dependence suggests that the larger particles do not extend as far from the ring plane. Also, well away from the ring plane the particle mass distribution on the inbound crossing showed a notable step-like decrease for particle radii greater than about 2–3 μm. This step-like decrease suggests that some local process may be acting to erode or modify the distribution of larger particles that are orbiting at inclined angles to the ring plane.

Acknowledgments

This research was supported by NASA through contract 961152 with the Jet Propulsion Laboratory.

References

Aubier, M.G., Meyer-Vernet, N., Pedersen, B.M., 1983. Shot noise from grain and particle impacts in Saturn's ring plane. Geophys. Res. Lett. 10, 5–8.

Esposito, L.W., Cuzzi, J.N., Holberg, J.B., Marouf, E.A., Tyler, G.L., Porco, C.C., 1984. Saturn's rings: structure, dynamics, and particle properties. In: Gehrels, T., Matthews, M.S. (Eds.), Saturn. University of Arizona Press, Tucson, pp. 463–545.

Grün, E., 1981. Experimental studies of impact ionization. European Space Agency Special Publication, ESA SP-155, pp. 81–90.

Gurnett, D.A., Grün, E., Gallagher, D., Kurth, W.S., Scarf, F.L., 1983. Micron-sized particles detected near Saturn by the Voyager plasma wave instrument. Icarus 53, 236–254.

Gurnett, D.A., Kurth, W.S., Kirchner, D.L., Hospodarsky, G.B., Averkamp, T.F., Zarka, P., Lecacheux, A., Manning, R., Roux, A., Canu, P., Cornilleau-Wehrlin, N., Galopeau, P., Meyer, A., Bostrom, R., Gustafsson, G., Wahlund, J.-E., Aahlen, L., Rucker, H.O., Ladreiter, H.-P., Macher, W., Woolliscroft, L.J.C., Alleyne, H., Kaiser, M.L., Desch, M.D., Farrell, W.M., Harvey, C.C., Louarn, P., Kellogg, P.J., Goetz, K., Pedersen, A., 2004. The Cassini radio and plasma wave science investigation. Space Sci. Rev. 114, 395–463.

Kempf, S., Srama, R., Horányi, M., Burton, M., Helfert, S., Moragas-Klostermeyer, G., Roy, M., Grün, E., 2005a. High-velocity streams of dust originating from Saturn. Nature 433, 289–291.

Kempf, S., Srama, R., Postberg, F., Burton, M., Green, S.F., Helfert, S., Hillier, J.K., McBride, N., McDonnell, J.A.M., Georg, M.K., Moragas-Klostermeyer, G., Roy, M., Grün, E., 2005b. Composition of Saturnian stream particles. Science 307, 1274–1276.

Kurth, W.S., Averkamp, T.F., Gurnett, D.A., Wang, Z., 2006. Cassini RPWS observations of dust in Saturn's E ring. Planet. Space Sci. this issue.

Matson, D.L., Spilker, L.J., Lebreton, J.-P., 2002. The Cassini/Huygens mission to the Saturnian system. Space Sci. Rev. 104, 1–58.

Scarf, F.L., Gurnett, D.A., Kurth, W.S., Poynter, R.L., 1982. Voyager 2 plasma wave observations at Saturn. Science 215, 587–594.

Smith, B.A., Soderblom, L., Beebe, R., Boyce, J., Briggs, G., Bunker, A., Collins, S.A., Hansen, C.J., Johnson, T.V., Mitchell, J.L., Terrile, R.J., Carr, M., Cook Jr., A.F., Cuzzi, J., Pollack, J.B., Danielson, G.E., Ingersoll, A., Davies, M.E., Hunt, G.E., Masursky, H., Shoemaker, E., Morrison, D., Owen, T., Sagan, C., Veverka, J., Strom, R., Suomi, V.E., 1981. Encounter with Saturn: Voyager 1 imaging science results. Science 212, 163–191.

Srama, R., Ahrens, T.J., Altobelli, N., Auer, S., Bradley, J.G., Burton, M., Dikarev, V.V., Economou, T., Fechtig, H., Görlich, M., Grande, M., Graps, A., Grün, E., Havnes, O., Helfert, S., Horanyi, M., Igenbergs, E., Jessberger, E.K., Johnson, T.V., Kempf, S., Krivov, A.V., Krüger, H., Mocker-Ahlreep, A., Moragas-Klostermeyer, G., Lamy, P., Landgraf, M., Linkert, D., Linkert, G., Lura, F., McDonnell, J.A.M., Möhlmann, D., Morfill, G.E., Müller, M., Roy, M., Schäfer, G., Schlotzhauer, G., Schwehm, G.H., Spahn, F., Stübig, M., Svestka, J., Tschernjawski, V., Tuzzolino, A.J., Wäsch, R., Zook, H.A., 2004. The Cassini cosmic dust analyzer. Space Sci. Rev. 114, 465–518.

Tsintikidis, D., Gurnett, D.A., Granroth, L.J., Allendorf, S.C., Kurth, W.S., 1994. A revised analysis of micron-sized particles detected near Saturn by the Voyager 2 plasma wave instrument. J. Geophys. Res. 99, 2261–2270.

Warwick, J.W., Pearce, J.B., Evans, D.R., Romig, J.H., Alexander, J.K., Desch, M.D., Kaiser, M.L., Aubier, M., Leblanc, Y., Lecacheux, A., Pedersen, B.M., 1982. Planetary radio astronomy observations from Voyager 2 near Saturn. Science 215, 582–587.